CrossMark

ORIGINAL CONTRIBUTION

Synthesis of polyaniline/CdS (nanoflowers and nanorods) nanocomposites: a comparative study towards enhanced photocatalytic activity for degradation of organic dye

Surbhi Sharma[1] · Simrjit Singh[1] · Neeraj Khare[1]

Abstract Cadmium sulfide nanoflowers (CdS-NF), nanorods (CdS-NR), and its nanocomposites with polyaniline (PANI) were successfully synthesized using facile chemical methods. Transmission electron microscopy (TEM) images confirmed the growth of CdS as nanoflowers and nanorods. High-resolution transmission electron microscopy (HRTEM) images showed clear lattice fringes, indicating good crystallinity of the CdS nanostructures and the formation of interface between PANI and CdS. The photocatalytic activity of CdS nanostructures and its composites was demonstrated for the degradation of methylene blue (MB) dye under visible light irradiation. The PANI/CdS nanocomposites showed enhancement in the photocatalytic activity as compared to bare CdS nanostructures, and it is attributed to efficient charge transfer between CdS and PANI. Photoluminescence study confirmed the enhancement in photogenerated electron–hole pairs separation in CdS nanostructures after the addition of PANI. The composite of PANI with CdS-NF exhibited larger improvement in the photodegradation efficiency over CdS-NF as compared to the improvement observed in PANI/CdS-NR over CdS-NR, which is attributed to the formation of more interfacial sites between PANI and CdS nanoflowers as compared to PANI and CdS nanorods. Our present work indicates that by carefully designing the semiconductor nanomaterial composites, the photocatalytic activity can be significantly enhanced.

Keywords CdS · Nanostructures · Nanocomposites · Polyaniline · Photocatalysis · Heterojunction

✉ Neeraj Khare
  nkhare@physics.iitd.ernet.in

[1] Department of Physics, Indian Institute of Technology Delhi, New Delhi 110016, India

Introduction

Organic dyes, which are being used in many industrial processes, have become a major source of water pollution and are creating severe environmental problems. Semiconductor photocatalysis is proven as a green energy technology for treating the industrial wastewater using the abundant solar energy. Various semiconductor materials such as TiO_2, ZnO, CdS, WO_3, etc., with different morphologies have been widely used as semiconductor photocatalysts for the degradation of organic dyes [1–4]. Among different semiconductor materials, photoactive CdS due to its direct band gap (~2.4 eV) and high absorption coefficient is a suitable material for visible light responsive photocatalytic applications [5]. But, the high recombination rate of the photogenerated electron–hole pairs reduces the photocatalytic efficiency of this material. To overcome this difficulty, several approaches such as the coupling of CdS with different semiconductor materials in the form of nanocomposites or as core/shell nanostructures have been used to improve the efficiency of semiconductor materials [6, 7].

Recently, the coupling of semiconductor materials with carbon nanostructures such as carbon nanotubes, graphene, and conducting polymers is also shown to be an effective strategy to improve the photocatalytic activity of the semiconductor materials due to their high electron mobility properties [8–12]. Among the conducting polymers, polyaniline (PANI) is a visible-light active semiconductor and consists of π conjugated system in which delocalization of π electrons leads to high conducting properties of this material [13, 14]. The coupling of PANI with various semiconductor materials, such as ZnO, $CoFe_2O_4$, TiO_2, and Bi_3NbO_7, etc., [15–20] has been reported for enhancing the photocatalytic activity.

In the present work, we report the synthesis of CdS nanorods and CdS nanoflowers by hydrothermal method and its coupling with polyaniline by a simple chemisorption method. The

photocatalytic activity of CdS nanostructures and its composites with PANI has been demonstrated for the degradation of methylene blue dye under visible light irradiation. The coupling of polyaniline with CdS nanostructures enhances the photocatalytic activity of both the CdS nanostructures; however, the rate of enhancement in the efficiency is found to be higher in PANI/CdS nanoflowers as compared to PANI/CdS nanorods. A reaction mechanism for the enhancement in the photocatalytic activity for the PANI-CdS nanocomposites has been proposed.

Experimental

Synthesis of polyaniline

PANI was synthesized by chemical oxidative polymerization of aniline [21]. A 0.5 l solution was prepared by adding 0.05 M of aniline and 0.5 M of HCl in deionized water stirred vigorously at 1 °C. After continuous stirring for 5 h, 0.05 M solution of ammonium peroxydisulphate was added dropwise to the above solution. The precipitates of conductive PANI (emeraldine salt form) were filtered and, finally, dried at 70 °C for 30 h. The powder was washed with ammonia solution to obtain an emeraldine base form of PANI.

Synthesis of CdS nanoflowers

CdS nanoflowers were synthesized by hydrothermal method. A 0.2 M of thiourea (CH_4N_2S) was added to 50 ml of deionized water and stirred for 10 min with rotation speed of 300 rpm. Cadmium nitrate ($Cd(NO_3)\cdot4H_2O$) was added to the above mixture and after continuous stirring for 30 min, the solution was placed into a Teflon-lined stainless steel autoclave at 180 °C for 12 h. The obtained precipitates were centrifuged and finally dried at 70 °C for 12 h.

Synthesis of CdS nanorods

CdS nanorods were synthesized by hydrothermal method [22]. A 2 mM cadmium nitrate ($Cd(NO_3).4H_2O$) was mixed in 30 ml of ethylenediamine ($NH_2CH_2CH_2NH_2$) and stirred for 20 min. Afterwards, the above solution was mixed with 8 mM of thiourea (CH_4N_2S) and stirred for 20 min with rotation speed of 300 rpm. The solution was kept into a Teflon-lined stainless steel autoclave at 170 °C for 12 h. The resultant precipitates were centrifuged and then dried at 70 °C for 12 h.

Synthesis of nanocomposites (PANI/CdS-NF, PANI/CdS-NR)

PANI/CdS-NF nanocomposite was synthesized by the simple chemisorption method. A 0.05 g PANI was added to 100 ml of tetrahydrofuran (THF) and stirred for 20 min with rotation

speed of 300 rpm. A certain amount of CdS-NF powder was added to the THF and PANI solution to synthesize 15 wt% of PANI/CdS nanocomposite. The mixture was ultrasonicated for 30 min. After vigorously stirring for 24 h, resultant precipitates were centrifuged and dried at 70 °C for another 24 h. PANI/CdS-NR was also synthesized by the same process as used for the synthesis of PANI/CdS-NF. PANI/CdS nanocomposites with different loading of PANI (5, 10, and 20 wt%) were also prepared. A schematic diagram for the synthesis of PANI and CdS nanocomposites is illustrated in Fig. 1.

Photocatalytic degradation experiment

The photocatalytic activity of CdS-NF, PANI/CdS-NF, CdS-NR, and PANI/CdS-NR was checked for the degradation of the methylene blue (MB) dye solution. A visible lamp (11 W) was used as a visible light source for performing the photodegradation experiment. The solution containing 0.1 g of photocatalyst powder in 250 ml of 1×10^{-5} M MB dye solution was ultrasonicated for 15 min and stirred for another 15 min in a dark atmosphere to reach equilibrium. The solution was collected in a 10-ml sample bottle before visible light illumination to determine initial concentration of MB. Afterwards, the solution was taken out at regular time intervals of visible light exposure. The concentration of MB was evaluated by taking the absorption spectra of the collected solution. Before taking the UV–vis spectra, the photocatalyst powder was removed from the dye solution through centrifuging and filtering the solution.

Characterization

X-ray diffraction of CdS nanostructures and its composites were performed by using Rigaku Ultima VI model diffractometer with CuK_α radiation ($\lambda = 1.54$ Å) in the 2θ range of 10–80°. Morphological studies were carried out by using Carl Zeiss EVO 50 series scanning electron microscope (SEM) and FEI Tecnai (accelerating voltage ~200 kV) transmission electron microscope. Fourier transform infrared (FTIR) spectra were measured using Thermo Scientific Nicolet 6700 spectrometer. Ultraviolet and visible (UV–vis) spectra were recorded by Perkin Elmer Lambda 1050 series dual-beam spectrophotometer. Photoluminescence (PL) spectra were recorded by using a Perkin Elmer LS 55 spectrometer with the excitation wavelength of ~325 nm.

Results and discussions

Structural analysis

Figure 2a illustrates the X-ray spectra (XRD) of PANI, CdS-NF, and PANI/CdS-NF (15 wt% loading of PANI). A broad

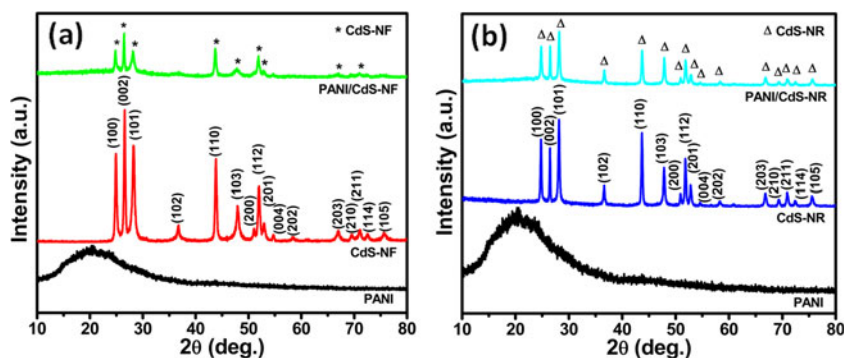**Fig. 1** Schematic diagram for the synthesis of PANI/CdS nanocomposites
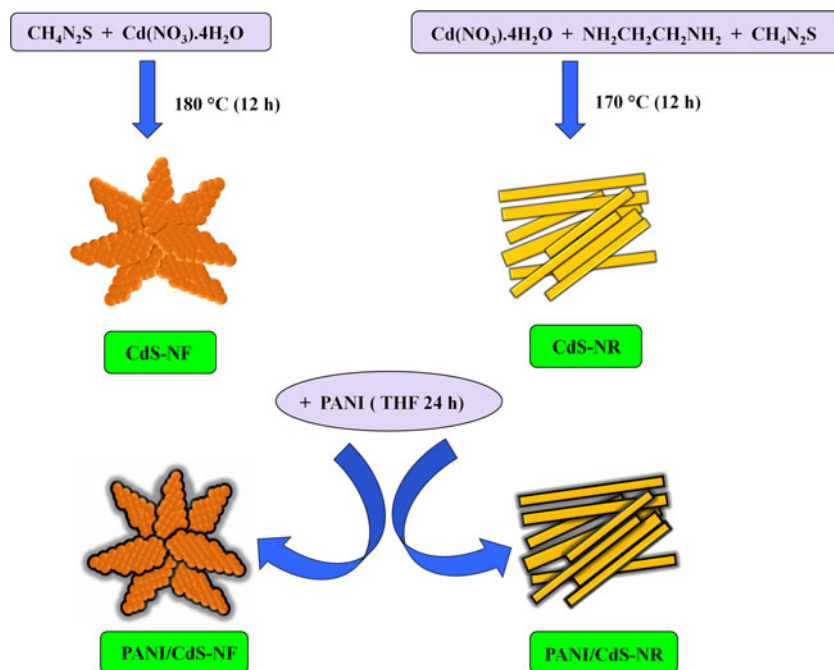
hump is observed between 10° and 35° in the XRD pattern of PANI which indicates the amorphous character of PANI. The sharp diffraction peaks of CdS-NF appeared at 2θ values 24.92°, 26.55°, 28.25°, 36.70°, 43.79°, 47.87°, 51.15°, 51.93°, 52.92°, 54.61°, 58.33°, 67.06°, 69.37°, 71.05°, 72.68°, and 75.76° corresponding to (100), (002), (101), (102), (110), (103), (200), (112), (201), (004), (202), (203), (210), (211), (114), and (105) planes of CdS, respectively (JCPDS file no. 41–1049) and signified high crystallinity of CdS-NF. The respective XRD peak positions of CdS-NF that were also seen in PANI/CdS-NF confirm that the crystal structure of CdS-NF has not been modified. Figure 2b shows the XRD patterns of PANI, CdS-NR, and PANI/CdS-NR (15 wt% loading of PANI). The XRD peaks of CdS-NR appeared at 24.79°, 26.46°, 28.15°, 36.59°, 43.68°, 47.82°, 50.89°, 51.83°, 52.80°, 54.46°, 58.33°, 66.82°, 69.27°, 70.93°, 72.37°, and 75.57° which confirms the formation of CdS-NR in pure hexagonal phase. The respective peaks of CdS-

NR also appear in PANI/CdS-NR, which clearly indicates the presence of both the phases in the nanocomposite structure.

Morphological studies

The morphologies of as synthesized CdS nanostructures and its composites were investigated by scanning electron microscopy (SEM). Figure 3 shows the morphology of CdS-NF, CdS-NR, and its composites with 15 wt% of PANI. The obtained CdS-NF and CdS-NR have been grown in the form of nanoflowers and nanorods (Fig. 3a, c). The coupling of PANI with CdS nanostructures is found on the surface as well as in between the CdS nanoflowers (Fig. 3b). However, in the case of CdS nanorods, the insertion of PANI brings morphological changes in CdS nanorods after adsorbing on its surface and boundaries (Fig. 3d). Figure 4 shows the transmission electron microscopy (TEM) and high-resolution transmission electron microscopy (HRTEM) images of CdS nanostructures and

Fig. 2 XRD patterns of **a** PANI, CdS-NF, and PANI/CdS-NF and **b** PANI, CdS-NR, and PANI/CdS-NR
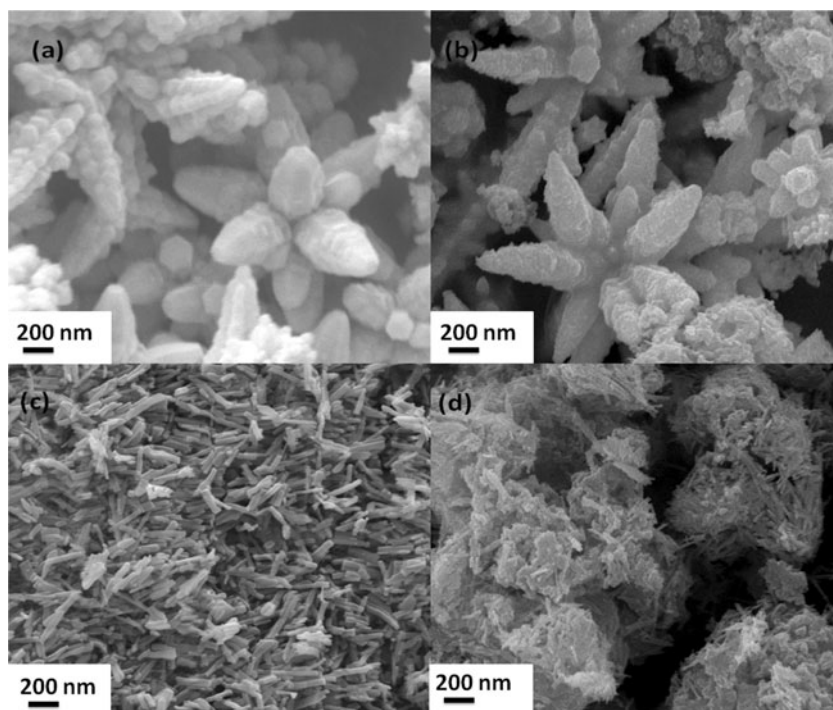
PANI/CdS (15 wt% PANI) nanocomposites. Figure 4a shows that CdS has been grown in the form of nanoflowers of length of several nanometers. In the HRTEM image, the interplanar spacing of CdS-NF is found to be ~0.358 nm corresponding to (100) plane (Fig. 4b). Figure 4c shows the loading of PANI on the surface and boundaries of CdS nanoflowers. The lattice fringes are also observed in PANI/CdS-NR, and the interplanar spacing is found to be ~0.358 nm corresponding to (100) plane (Fig. 4d). Figure 4e shows the TEM image of CdS grown in the form of nanorods with an aspect ratio of ~5.73. Figure 4f shows the clear lattice fringes of CdS nanorods indicating high crystallinity of prepared sample and the interplanar spacing between the planes is measured to be 0.358 nm corresponding to (100) plane. Figure 4g shows that PANI is adsorbed on the surface of nanorods. Figure 4h shows the lattice fringes in PANI/CdS-NR which reveals that the crystallinity of CdS nanorods is not affected after coupling with PANI, and the measured interplanar spacing is 0.358 nm corresponding to (100) plane.

FTIR studies

Figure 5a shows the FTIR spectra of PANI, CdS-NF, and PANI/CdS-NF (15 wt% PANI).The corresponding peaks of PANI are observed at 829 cm^{-1} (C–H bonding), 1106 cm^{-1} (C–H bonding of benzoid rings), 1230 cm^{-1} (C–N stretching of quinoid rings), 1308 cm^{-1} (C–N stretching of benzoid rings), 1381 cm^{-1} (C–N stretching of quinoid rings), 1500 cm^{-1} (C=C stretching of benzoid

rings), and 1587 cm^{-1} (C=C stretching of quinoid rings) [21, 23]. The peaks appeared at 503, 1106, 1230, and 1587 cm^{-1} corresponding to PANI that are shifted to higher wavenumbers 505, 1165, 1303, and 1589 cm^{-1}, respectively, in PANI/CdS-NF, while the peaks at 1308, 1381, and 1500 cm^{-1} are shifted to lower wavenumbers to 1303, 1375, and 1497 cm^{-1}, respectively. Figure 5b illustrates the FTIR studies of PANI, CdS-NR, and PANI/CdS-NR (15 wt% PANI). The peaks of PANI at 503, 1106, 1230, and 1587 cm^{-1} are shifted to higher wavenumbers 511, 1164, 1234, and 1589 cm^{-1}, respectively, in PANI/CdS-NR. While the peaks at 1308, 1381, and 1500 cm^{-1} are shifted to lower wavenumbers to 1303, 1376, and 1497 cm^{-1}. The shift in the characteristic peaks of PANI in the PANI/CdS nanocomposites confirms an interaction between of CdS nanostructures with the molecular chains of PANI.

Optical studies

Figure 5c–d shows UV–vis absorption spectra of PANI, CdS-NF, CdS-NR, PANI/CdS-NF (15 wt% PANI), and PANI/CdS-NR (15 wt% PANI). For the PANI, the characteristic absorption maxima at ~600 nm is due to π to π^* transition in benzoid units and formation of polaron in emeraldine base form of PANI [24]. The absorption maxima of both CdS-NF and CdS-NR are observed at ~490 nm which corresponds to an optical band gap (E_g) of ~2.53 eV. Thus, the change in the

Fig. 4 TEM images of **a** CdS-NF, **c** PANI/CdS-NF, **e** CdS-NR, and **g** PANI/CdS-NR and HRTEM images of **b** CdS-NF, **d** PANI/CdS-NF, **f** CdS-NR, and **h** PANI/CdS-NR
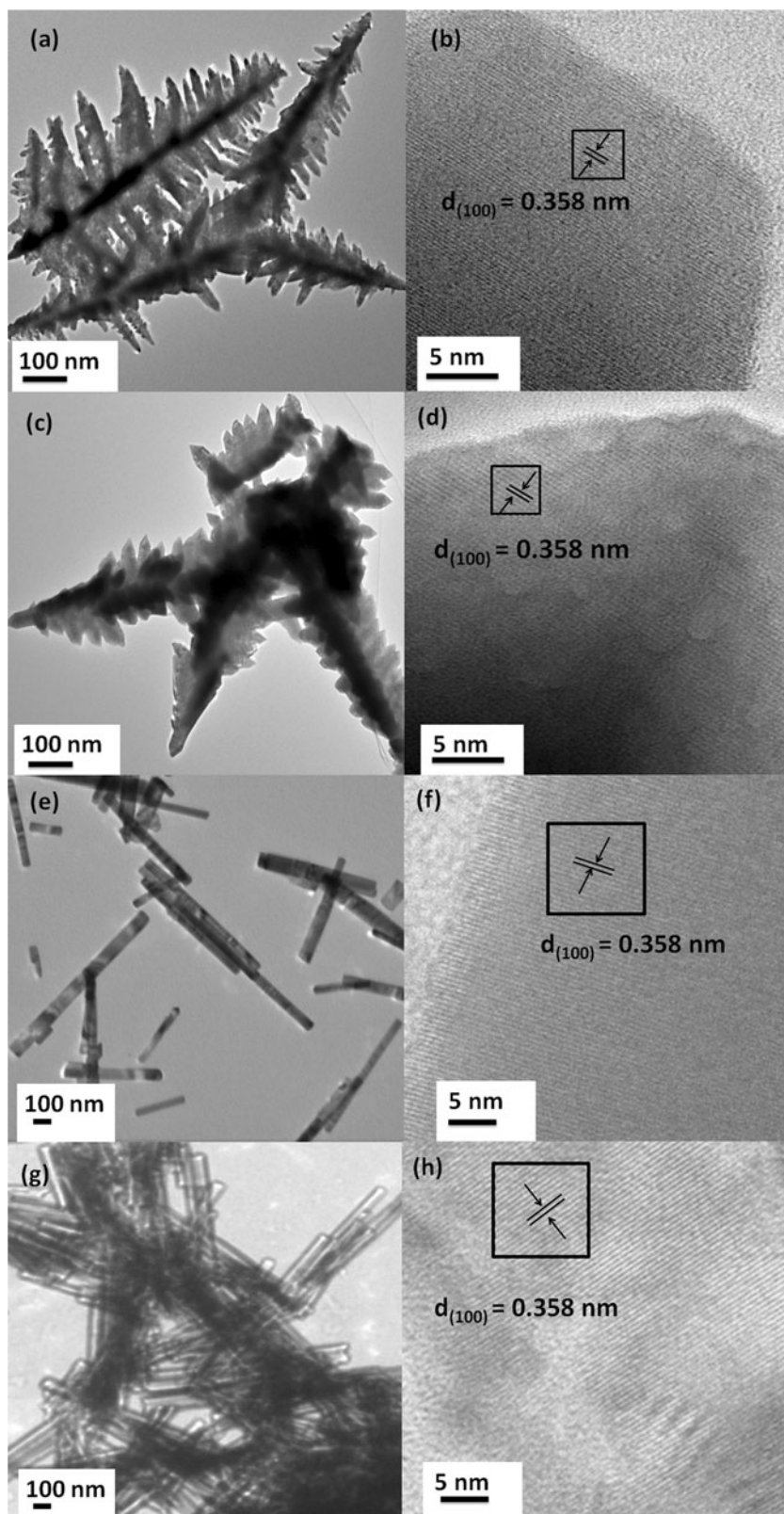
morphology of CdS does not alter its band gap. However, after coupling with PANI, the band gap of CdS shifts towards a higher wavelength of ~504 nm.

The reduction in the band gap of PANI/CdS-NR and PANI/CdS-NF can be due to the formation of defect states in CdS after coupling with PANI.
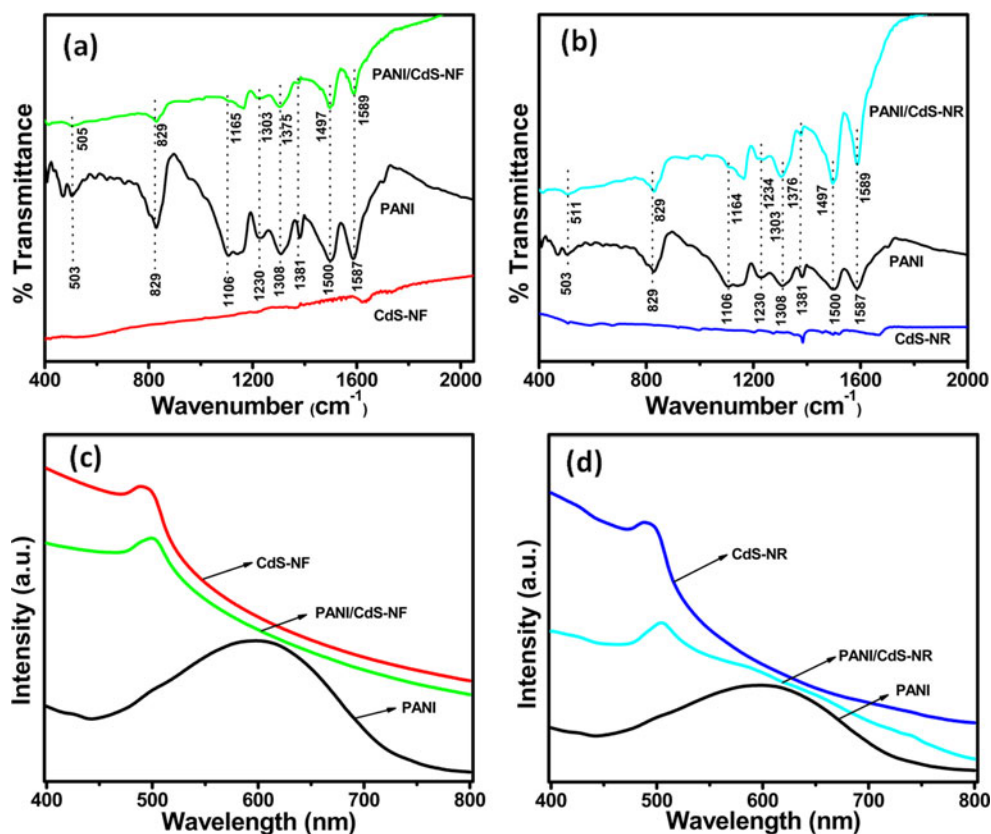
Photocatalytic degradation of MB dye

Figure 6a–b illustrates UV–vis absorption spectra of MB solution after exposure to visible light in the presence of PANI/CdS-NF and PANI/CdS-NR photocatalysts (15 wt% PANI) respectively. The MB concentration in the solution is determined from the maxima of the optical absorption spectra. The absorption peak of MB decreases gradually, confirming its degradation due to the photocatalytic reaction of different nanostructure photocatalysts after visible light exposure. The inset of Fig. 5a–b shows gradual disappearance of initial MB color. Figure 6c–d shows a comparison of relative concentration of the MB and reaction rate constant in the presence of CdS-NF, PANI/CdS-NF, CdS-NR, and PANI/CdS-NR. The reaction rate constant is determined by the pseudo first-order kinetics reaction [12]

$$\ln\frac{C_0}{C} = kt$$

where C_0 is the initial MB concentration, C is the concentration after a time interval, and k is the reaction rate constant. The reaction rate constant is obtained as 0.161, 0.304, 0.287, and 0.379 h^{-1} in the presence of CdS-NF, PANI/CdS-

NF, CdS-NR, and PANI/CdS-NR, respectively (Fig. 6e). The photocatalytic activity of both the nanostructures of CdS gets enhanced after coupling with PANI in PANI/CdS nanocomposite. It is also observed that bare CdS-NR shows a higher photocatalytic activity than CdS-NF, but after incorporating with conducting polymer PANI, the nanocomposite PANI/CdS-NF has shown larger improvement in the photocatalytic activity as compared to PANI/CdS-NR which is attributed to the formation of more interfacial sites between PANI and CdS-NF. The rate constant of PANI/CdS-NF is enhanced by ~1.9 times over pure CdS-NF whereas the rate constant of PANI/CdS-NR is enhanced by ~1.3 times over CdS-NR. To see the effect of loading concentration of PANI on the photocatalytic activity of PANI/CdS nanocomposites, we have prepared different samples of the PANI/CdS nanocomposites by taking different weight percentages of the PANI (5, 10, 15, and 20 wt%). The photocatalytic activity of the PANI/CdS nanocomposite increases with increasing the loading percentage (5, 10, and 15 wt%) of PANI in the nanocomposite due to the efficient transfer of the charge carriers between PANI and CdS nanostructures leading to decrease in the recombination rate of the photogenerated charge carriers. However, the photocatalytic activity was found to reduce when 20 wt% of PANI was

Fig. 6 UV–vis absorption spectra of MB solution in the presence of **a** PANI/CdS-NF, **b** PANI/CdS-NR after different time of visible light exposure, the *inset* shows change in the color of MB solution after different irradiation time. Variation of concentration of MB (C/C_0) vs. time plot in the presence of **c** CdS-NF and PANI/CdS-NF, **d** CdS-NR and PANI/CdS-NR, and **e** comparison of rate constants of CdS-NF, PANI/CdS-NF, CdS-NR, and PANI/CdS-NR
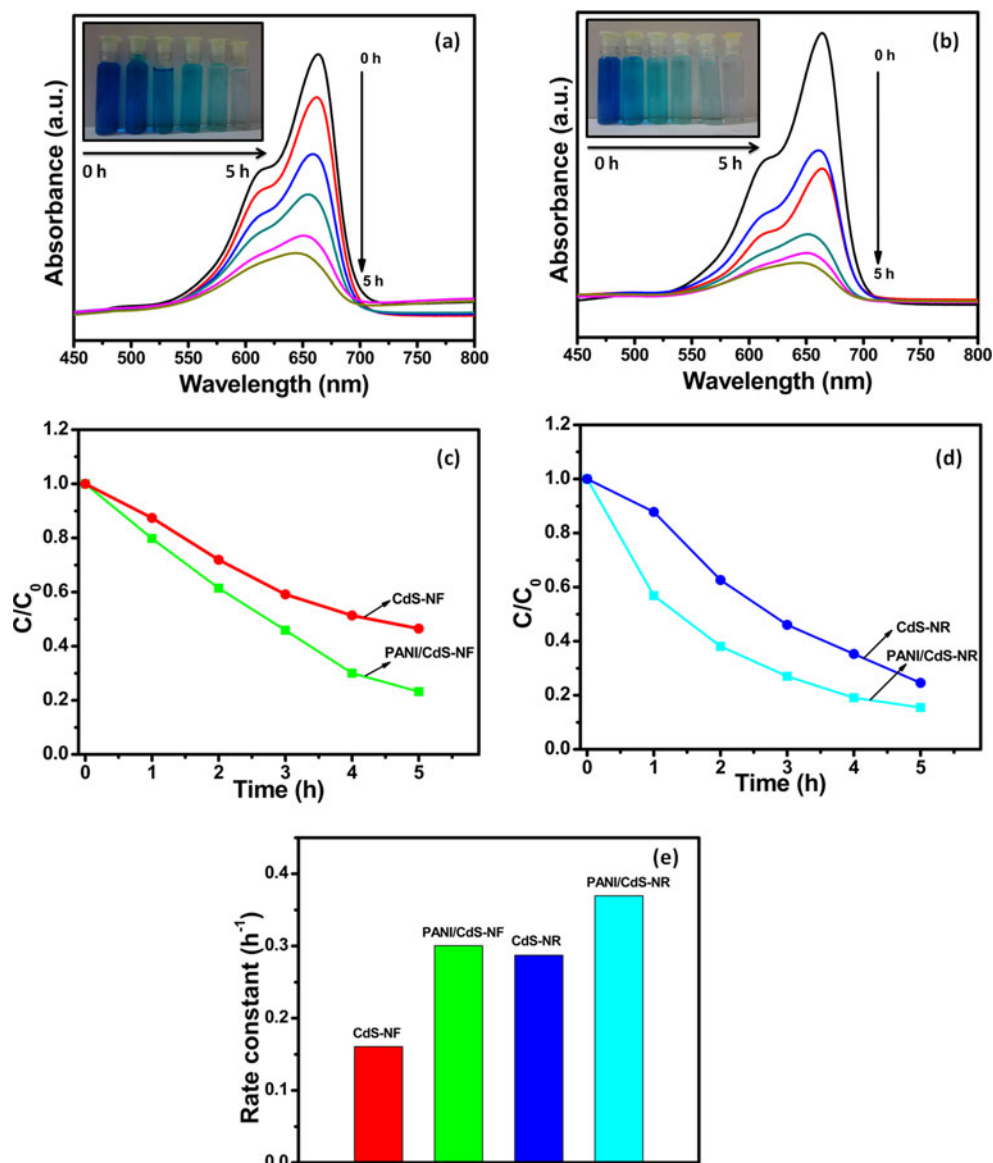
used in PANI/CdS nanocomposite. It seems that the higher amount of the PANI in the nanocomposite tends to accumulate on the surface of the CdS nanostructures leading to a reduction in the photocatalytic activity.
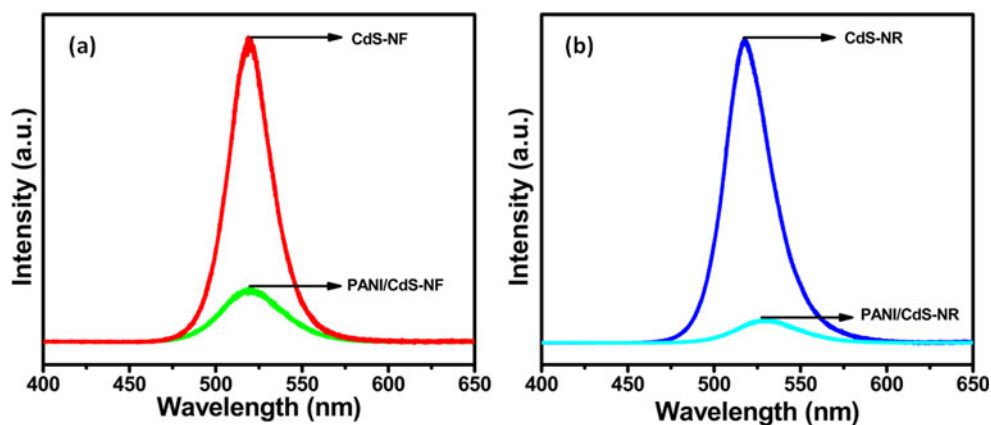
Photoluminescence studies

Figure 7 shows the photoluminescence spectra of CdS-NF, CdS-NR, PANI/CdS-NF (15 wt% PANI), and PANI/CdS-NR (15 wt% PANI) for the excitation wavelength of 325 nm. The maximum of PL emission peak for CdS-NF and CdS-NR is observed at ~518 nm corresponding to interband electron–hole recombination [25, 26]. The PL intensity decreases in PANI/CdS nanocomposites, which confirms that PANI plays crucial role in

separating the charge carriers significantly. Formation of type II heterojunction between PANI and CdS facilitates the photogenerated charge carrier separation which resulted in the enhanced photocatalytic activity of CdS nanostructures after addition of PANI.
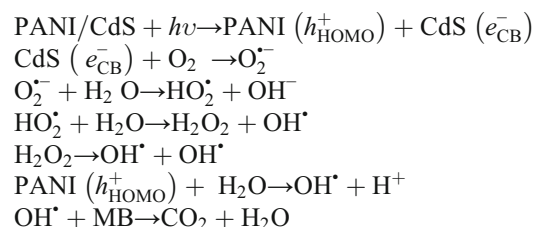
Mechanism

The possible mechanism for the MB degradation under visible-light exposure was proposed by the schematic band diagram of PANI/CdS nanocomposite (Fig. 8). The conduction band (CB) of CdS (~ -0.8 eV w.r.t. NHE) [27] lies below the LUMO level of PANI (~ -1.9 eV w.r.t. NHE) [28], and the valence band (VB) of CdS (~1.6 eV

w.r.t. NHE) lies below the HOMO level (~0.8 eV w.r.t. NHE) of PANI forming type II heterojunction between PANI and CdS. Under visible light illumination, both CdS and PANI get photoexcited and photoinduced electrons from LUMO level of PANI and are transferred to the CB of CdS, and the holes from the VB of CdS are injected to the HOMO level of PANI. The transferred photogenerated electrons in the CB of CdS react with the adsorbed O_2 to generate reactive superoxide anion $(O_2^{\bullet-})$ radicals. These $O_2^{\bullet-}$ radicals further react with water molecules and undergo secondary reactions to produce hydroxyl radicals $(OH^{\bullet})$. Simultaneously, photoinduced holes in the HOMO level of PANI react with water molecules to produce $OH^{\bullet}$ radicals through oxidation reaction. Finally, the highly reactive $OH^{\bullet}$ radicals react with MB

molecules and dissociate it into CO_2 and H_2O byproducts. The possible photocatalytic reaction mechanism for photodegradation of MB is described as

$$PANI/CdS + h\upsilon \rightarrow PANI\left(h^+_{HOMO}\right) + CdS\left(e^-_{CB}\right)$$
$$CdS\left(e^-_{CB}\right) + O_2 \rightarrow O_2^{\bullet-}$$
$$O_2^{\bullet-} + H_2O \rightarrow HO_2^{\bullet} + OH^-$$
$$HO_2^{\bullet} + H_2O \rightarrow H_2O_2 + OH^{\bullet}$$
$$H_2O_2 \rightarrow OH^{\bullet} + OH^{\bullet}$$
$$PANI\left(h^+_{HOMO}\right) + H_2O \rightarrow OH^{\bullet} + H^+$$
$$OH^{\bullet} + MB \rightarrow CO_2 + H_2O$$

The incorporation of PANI in CdS nanostructures facilitates faster transfer of charge carriers at the interface and thereby reducing electron–hole pairs recombination rate. The
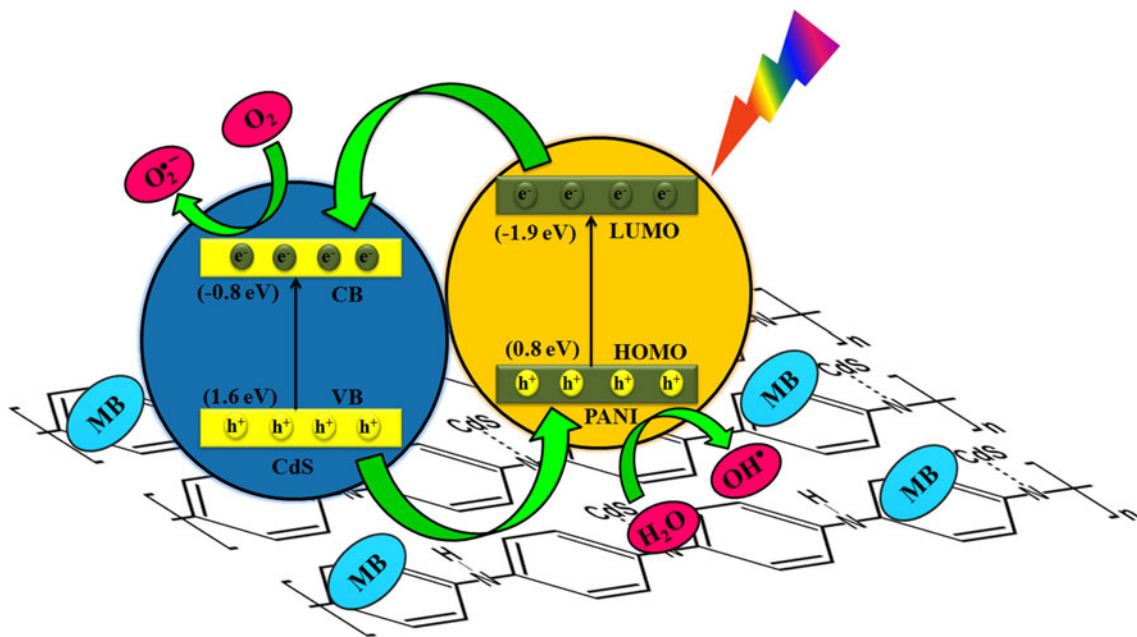
Fig. 8 Schematic band diagram of PANI/CdS nanocomposite showing the possible photocatalytic reaction mechanism for the degradation of MB under visible light illumination

higher separation of photogenerated charge carriers in turn enhances the formation of hydroxyl and superoxide radicals and finally degrades the dye molecules at a faster rate. Therefore, the photocatalytic activity of semiconductor material increases due to the hybrid effect between PANI and CdS nanostructures.

Conclusions

In conclusion, CdS with two different morphologies (nanoflowers, nanorods) was synthesized and it was found that the CdS nanorods exhibit higher photocatalytic activity as compared to CdS nanoflowers which reveals that the photocatalytic activity depends upon the morphology of the semiconductor nanostructures. Furthermore, the CdS nanostructures were coupled with conducting polymer polyaniline and an enhancement in the photocatalytic activity due to the formation of type II heterojunction between the CdS and polyaniline was demonstrated. In comparison to PANI/CdS-NR, larger improvement in the photodegradation efficiency was observed in PANI/CdS-NF over CdS-NF which is attributed to the formation of more interfacial sites between CdS nanoflowers and PANI leading to higher separation efficiency of the photogenerated charge carriers.

References

1. Joo JB, Lee I, Dahl M, Moon GD, Zaera F, Yin Y (2013) Controllable synthesis of mesoporous TiO_2 hollow shells: toward an efficient photocatalyst. Adv Funct Mater 23:4246–4254

2. Gupta J, Barick KC, Bahadur D (2011) Defect mediated photocatalytic activity in shape-controlled ZnO nanostructures. J Alloys Compd 509:6725–6730

3. Huang Y, Sun F, Wu T, Wu Q, Huang Z, Su H, Zhang Z (2011) Photochemical preparation of CdS hollow microspheres at room temperature and their use in visible-light photocatalysis. J Solid State Chem 184:644–648

4. Adhikari S, Sarkar D, Madras G (2015) Highly efficient WO_3–ZnO mixed oxides for photocatalysis. RSC Adv 5:11895–11904

5. Wang C, Lin H, Xu Z, Cheng H, Zhang C (2015) One-step hydrothermal synthesis of flowerlike MoS_2/CdS heterostructures for enhanced visible-light photocatalytic activities. RSC Adv 5: 15621–15626

6. Singh S, Khare N (2015) Magnetically separable, $CoFe_2O_4$ decorated CdS nanorods for enhanced visible light driven photocatalytic activity. Mater Lett 161:64–67

7. Singh S, Khare N (2015) CdS/ZnO core/shell nano-heterostructure coupled with reduced graphene oxide towards enhanced photocatalysis activity and photostability. Chem Phys Lett 634: 140–145

8. Wang Z, Yin L, Zhang M, Zhou G, Fei H, Shi H, Dai H (2014) Synthesis and characterization of Ag_3PO_4/multiwalled carbon nanotube composite photocatalyst with enhanced photocatalytic activity and stability under visible light. J Mater Sci 49:1585–1593

9. Fang R, Liang Y, Ge X, Du M, Li S, Li T, Li Z (2015) Preparation and photocatalytic degradation activity of TiO_2/rGO/polymer composites. Colloid Poly Sci 293:1151–1157

10. Yang Y, Li E, Fan J, Hu X, Hou W, Wu F, Ma Y (2014) A green and facile microwave-assisted synthesis of TiO_2/graphene nanocomposite and their photocatalytic activity for methylene blue degradation. J Phys Chem A 88:478–483

11. Ameen S, Akhtar MS, Kim YS, Yang OB, Shin HS (2011) An effective nanocomposite of polyaniline and ZnO: preparation, characterizations, and its photocatalytic activity. Colloid Poly Sci 289: 415–421

12. Medina VMO, López RG, Reyes BEC, Dávila PAA, Gutiérrez HM, Ortega OG, Cepeda LF (2015) Composite of acicular rod-like ZnO nanoparticles and semiconducting polypyrrole photoactive under visible light irradiation for methylene blue dye photodegradation. Colloid Poly Sci. doi:10.1007/s00396-015-3717-2

13. Rivera MAC, Medina VMO, Gutiérrez HM, Aguilar FES, Pérez E, Carmona IDA (2015) Morphology and conductivity tuning of polyaniline using short-chain alcohols by heterophase polymerization. Colloid Poly Sci 293:605–615

14. Rahman MA, Kumar P, Park DS, Shim YB (2008) Electrochemical sensors based on organic conjugated polymers. Sensors 8:118–141

15. Eskizeybek V, Sari F, Gülce H, Gülce A, Avci A (2012) Preparation of the new polyaniline/ZnO nanocomposite and its photocatalytic activity for degradation of methylene blue and malachite green dyes under UV and natural sun lights irradiations. Appl Catal B: Environ 119–120:197–206

16. Zhang H, Zong R, Zhu Y (2009) Photocorrosion inhibition and photoactivity enhancement for zinc oxide via hybridization with monolayer polyaniline. J Phys Chem C 113:4605–4611

17. Xiong P, Chen Q, He M, Sun X, Wang X (2012) Cobalt ferrite–polyaniline heteroarchitecture: a magnetically recyclable photocatalyst with highly enhanced performances. J Mater Chem 22:17485–17493

18. Li X, Teng W, Zhao Q, Wang L (2011) Efficient visible light-induced photoelectrocatalytic degradation of rhodamine B by polyaniline-sensitized TiO_2 nanotube arrays. J Nanoparticle Res 13:6813–6820

19. Zhang H, Zong R, Zhao J, Zhu Y (2008) Dramatic visible photocatalytic degradation performances due to synergetic effect of TiO_2 with PANI. Environ Sci Technol 42:3803–3807

20. Wu W, Liang S, Shen L, Ding Z, Zheng H, Su W, Wu L (2012) Preparation, characterization and enhanced visible light photocatalytic activities of polyaniline/Bi_3NbO_7 nanocomposites. J Alloys Compd 520:213–219

21. Sharma BK, Khare N, Dhawan SK, Gupta HC (2009) Dielectric properties of nano ZnO-polyaniline composite in the microwave frequency range. J Alloys Compd 477:370–373

22. Singh S, Khare N (2015) Reduced graphene oxide coupled CdS/$CoFe_2O_4$ ternary nanohybrid with enhanced photocatalytic activity and stability: a potential role of reduced graphene oxide as a visible light responsive photosensitizer. RSC Adv 5:96562–96572

23. Ozkazanc E, Zor S, Ozkazanc H, Guney HY, Abaci U (2012) Synthesis, characterization and dielectric behavior of (ES)-form polyaniline/cerium(III)-nitrate-hexahydrate composites. Mater Chem Phys 133:356–362

24. He K, Li M, Guo L (2012) Preparation and photocatalytic activity of PANI-CdS composites for hydrogen evolution. Int J Hydrog Energy 37:755–759

25. Chen F, Qiu W, Chen X, Yang L, Jiang X, Wang M, Chen H (2011) Large-scale fabrication of CdS nanorod arrays on transparent conductive substrates from aqueous solutions. Sol Energy 85:2122–2129

26. Zhao JG, Hua ZH, Yau Y (2013) Solvothermal synthesis and characterization of one-dimensional CdS nanowires. Superlattice Microst 61:146–151

27. Sasikala R, Shirole AR, Sudarsan V, Girija KG, Rao R, Sudakar C, Bharadwaj SR (2011) Improved photocatalytic activity of indium doped cadmium sulfide dispersed on zirconia. J Mater Chem 21:16566–16573

28. Wang Q, Hui J, Li J, Cai Y, Yin S, Wang F, Su B (2013) Photodegradation of methyl orange with PANI-modified BiOCl photocatalyst under visible light irradiation. Appl Surf Sci 283:577–583